Integrated Ferroelectrics, 2002, Vol. 43, pp. 51–64
Reprints available directly from the publisher
Photocopying permitted by license only

© 2002 Taylor & Francis
DOI: 10.1080/10584580190043705

An Alternative Route for the Synthesis of Oriented $LiNbO_3$ Thin Films

V. BORNAND,[a,*] I. HUET,[a] J. F. BARDEAU,[b] D. CHATEIGNER,[b] and Ph. PAPET[a]

[a]*Laboratoire de Physicochimie de la Matière Condensée UMR CNRS 5617, UM II Place Eugène Bataillon, C.C.003, F-34095 MONTPELLIER Cedex 5, France*
[b]*Laboratoire de Physique de l'Etat Condensé UPRES A 6087, Université du Maine, Avenue Olivier Messiaen, F-72085 LE MANS Cedex 9, France*

(Received March 22, 2001)

A new 2-step growth process was developed, combining both the r.f. sputtering and the pyrosol techniques, in which nucleation and growth stages could be partially separated and controlled. Using this refined deposition method, $\langle c \rangle$-oriented $LiNbO_3$ thin films could be successfully grown on (111) silicon and (001) sapphire substrates. Thin film structures have been determined by X-ray diffraction and pole figure analyses. Depositions performed on Si (111) templates led to fiber textures, characteristic of oriented polycrystalline samples. Al_2O_3 (001) substrates allowed the growth of in-plane oriented layers with two distinguishable variants in the interfacial plane, namely, an aligned variant $\langle 110 \rangle LiNbO_3 // [110]Al_2O_3$ and a 60°-rotated one.

Keywords: $LiNbO_3$ thin films; r.f. sputtering; pyrosol; 2-step growth; texture; pole figures

INTRODUCTION

Surface acoustic wave (SAW) devices are critical components for the wireless-communication industry where they are used in a wide variety of high-frequency filtering or wave-guiding applications. As a response to the increasing demands for large-volume data transmission and mobile communication, materials in the (3 m) crystallographic class have received a significant attention these last few years because of their unusual combination of ferroelectric, optical, elastic and piezoelectric properties. Among these systems, lithium niobate ($LiNbO_3$) is getting a growing technological

*Corresponding author.

importance for both integrated and active guided-wave applications. Its diversity of large-magnitude physical properties [1–6] has caused $LiNbO_3$ to become widely used in various micro-electronic and micro-optic devices, whether as resonators for electromechanical filter applications and acoustic delay lines, or as optical modulators and dielectric waveguides. If these applications are currently implemented on bulk materials, $LiNbO_3$ thin films deposited on appropriately-selected substrates should enable not only large electromechanical coupling constants but also high SAW velocity and good temperature coefficients [7–10].

In many devices, it is necessary to grow $LiNbO_3$ films with a preferred crystallographic orientation, in order to couple the large electro-optical and non-linear optical coefficients with the main piezoelectric constants along a favorable direction, i.e. with the *c*-axes normal to the surface of the substrate. Different approaches and techniques have been used for the preparation of well-ordered films, including both chemical and physical deposition methods. However, controlling the surface crystallization to obtain oriented films with the expected crystalline phase is usually difficult. That is why current research efforts are now focused on increasing the film quality in terms of crystallinity, topography, homogeneity, to form sufficiently-piezoelectric heterostructures for the effective fabrication of high-performance SAW devices.

Recently, we have developed a new 2-step deposition process devoted to the growth of highly-oriented $LiNbO_3$ thin films [11, 12]. This process involves (1) creating a high-nucleation density by r.f. sputtering in the early stages of the film growth and (2) enhancing both the crystallinity and the preferential orientation by reactive chemical sputtering (commonly named pyrosol). Using this refined growth process, combining both a physical and a chemical deposition technique, homogeneous and strongly $\langle 001 \rangle$-oriented $LiNbO_3$ thin films could be obtained on Si-(111) substrates. In this paper, we extend this work and provide additional insight for the in-plane organization of the as-deposited layers on (111)-oriented silicon and (001)-oriented sapphire single-crystal substrates. The structural characteristics, including morphology, topography and hetero-epitaxial relationships are quantitatively analyzed. Expected SAW velocities (V_s) and electromechanical coupling coefficients (K^2) are calculated for the as-grown films, and correlated to their microstructural state.

EXPERIMENTAL PROCEDURE

A detailed description of the r.f. sputtering and pyrosol processes can be found elsewhere, along with a comprehensive study of the best deposition

TABLE I Growth conditions of $LiNbO_3$ films deposited by a combined-deposition process

(a) Step 1: r.f. sputtered layer		(b) Step 2: pyrosol deposited layer	
Targets	Sintered ceramics Li/Nb = 1.4	Precursors	Li(AA) + $Nb(Et)_4$
		Solvent	Methanol
Gas	Mix Ar:O_2 (60:40)	Solutions	[Li] = 10^{-2} mol/l−Li/Nb = 1
Pressure	20 to 60 m Torr	Spraying	f = 800Hz−P = 70 W
r.f. Power	100 W	Carrier gas	Dry and clean air
Temperature	600 to 625 °C	Temperature	600 to 660 °C

conditions [12]. The depositions were performed at a temperature high enough to ensure the in-situ crystallization of the films. A summary of the experimental processing conditions is presented in Table I. Both Si-(111) and Al_2O_3-(001) were used as substrates for the elaboration of oriented thin films (Table II). Controlled growth on silicon potentially offers to combine the piezoelectric and optical processing capabilities of $LiNbO_3$, and the obvious electronic advantages of Si. Concerning sapphire substrates, its similar lattice parameters compared to $LiNbO_3$ as well as the large propagation velocities ($V_s \sim 5700$ m/s) that can be achieved on such a template, should allow the hetero-epitaxial growth of piezoelectric and SAW efficient thin films.

The structural characteristics of the films were investigated by X-ray diffraction (XRD) on a standard powder diffractometer using $Cu_{K\alpha}$ averaged radiation in the Bragg-Brentano geometry. In addition to the usual $\theta-2\theta$ scans, ω-scans (i.e. rocking curve experiments) for the $LiNbO_3$ (006) peak were recorded to evaluate the angular dispersion around the growth axis and, qualitatively, the crystalline quality. Full Widths at Half Maxima (FWHM) were determined by fitting the experimental curve with a Gaussian function. In order to study the in-plane orientation of optimized samples, we used Quantitative Texture Analyses (QTA) on a 4-circle diffractometer equipped with a curved position sensitive detector which spans all the necessary pole figures at once. The experimental set, corrections for background, defocusing, absorption and volume variations were described elsewhere [13,14], so

TABLE II Structure, lattice parameters and thermal expansion coefficients of $LiNbO_3$, Al_2O_3 and Si (data from ASTM standards)

Structure			a (Å)	c (Å)	$\alpha_{\perp c}$ (10^6/°C)	$\alpha_{//c}$ (10^6/°C)
$LiNbO_3$	Hexagonal (Rhomboedral)	R3c	5.1494	13.862	16.7	2
Al_2O_3	Hexagonal (Rhomboedral)	R$\bar{3}$c	4.758	12.991	4.5	5.3
Si	Cubic	Fd3m	5.430		4.2	4.2

was the quantifying methodology for integration and volumic proportion calculations [15]. The refinement of the Orientation Distribution Function (ODF), which allows the recalculation of the complete pole figures from the incomplete measured ones, was operated using the WIMV algorithm of Beartex [16]. The film surface morphology and topography were observed by Scanning Electron Microscopy (SEM) and Atomic Force Microscopy (AFM). Secondary Ion Mass Spectrometry (SIMS) depth profiling was used to assess both film composition and interdiffusion phenomena.

To measure the SAW properties, standard interdigital transducer (IDT) circuits (finger width/finger space $\sim$0.5) were fabricated on the surface of the as-grown films. Experimental SAW measurements were collected by a network analyzer while theoretical SAW characteristics (SAW velocities V_s and electro-mechanical coupling coefficients K^2) were calculated by the Fahmy and Adler method [17, 18].

RESULTS AND DISCUSSION

Microstructural Properties

As already demonstrated in a previous work [12], the final quality of the films strongly depends on the used substrates. In the present deposition process, the first weakly-crystallized sputtered film acts as a coherent buffer layer for the overall pyrosol-deposited film, thus (1) enhancing the growth of strongly-oriented crystallites, (2) limiting the surface roughness and (3) resulting in fine columnar grain structures. Under optimized conditions, highly $\langle c \rangle$-oriented films can be obtained on Al_2O_3-(001) and on Si(111) substrates. Both XRD and rocking curve analyses confirm the strong orientation and the high crystalline quality of the as-deposited layers (Fig. 1). The sapphire substrate, by itself, has a 0.05° FWHM for the same geometry. On Al_2O_3-(001) substrates (Fig. 1b), one can see that several orientation components are present, such as (110) and (006), which means that part of the material is also oriented with (110)-planes parallel to the sample plane, though it is a minor component. Besides, many small peaks are also present that can be indexed as secondary Li-deficient phases arising from the high-temperature deposition process.

Based on their similar packing structure of atoms giving rise to coincidence site lattices, as well as on the partial ionic character of $LiNbO_3$ [19, 20] reducing the effect of interfacial restrictions, highly oriented $LiNbO_3$ thin films are expected to be grown on sapphire. Indeed, despite (1) the relatively large mismatch with the substrate ($\sim$8% along the [100] direction) and

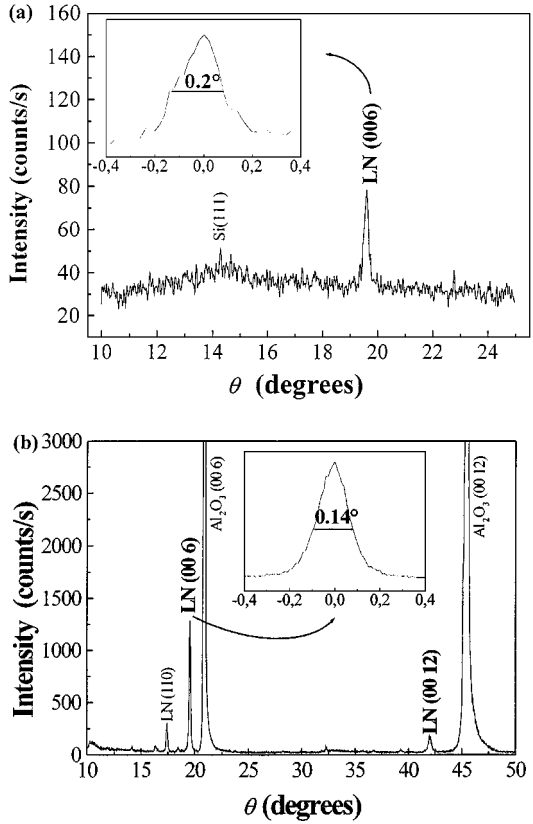

FIGURE 1 XRD patterns of $LiNbO_3$ thin films deposited by the combined-deposition process on **(a)** Si (111) and **(b)** Al_2O_3 (001) substrates. Insert shows the $LiNbO_3$ (006) rocking curve.

(2) the presence of misoriented (110) grains (extra peak at $\theta \sim 17.41^\circ$), they exhibit a marked preferential orientation along the $\langle 001 \rangle$ direction as shown by the high values of the $f(006)$ Lotgering factor [21] around 0.90, as calculated from the $LiNbO_3(00l)$ peaks (Fig. 1b). However, classical XRD is not able to reveal eventual in-plane orientation, which would be the signature of an hetero-epitaxial stabilization of the films. A perfect $\langle 001 \rangle$ fiber texture or an in-plane oriented film would exhibit the same (006) rocking curve, and could show the same θ–2θ diagram.

Concerning silicon templates, one theoretical explanation for how preferentially-oriented thin films may be produced on substrates without the

influence of hetero-epitaxy (such as cubic Si for rhombohedral $LiNbO_3$) centers on the role that plays surface energy in controlling the crystal growth speed [22–24]. Following the common nucleation-coalescence-growth model during the deposition, the islands of material with the lowest surface energy, that nucleate during the initial growth stages, enlarge over the critical size and grow to continue to reduce the free energy. Close packed planes, such as the (111) plane in the face-centered cubic structure of Si, exhibit the highest density of nucleation centers, which should enhance the first stages of the deposition process. Then, it is possible that films with low surface energy and corresponding texture, such as ⟨001⟩-oriented $LiNbO_3$ layers (Fig. 1a), are more easily stabilized during equilibrium deposition conditions on such oriented substrates [22, 23]. However, there are no data available to distinguish the planes with the lowest energy in $LiNbO_3$ crystals.

An other explanation for this preferential alignment of the $LiNbO_3$ crystallites on Si-(111) lies in symmetrical considerations. Since the ⟨*c*⟩-axis of $LiNbO_3$ and the ⟨111⟩-orientation of Si both exhibit a 3-fold symmetry and despite the presence of an amorphous SiO_2 native oxide layer ($<$50 Å) at the surface of the heated substrate, growth should be initiated in this direction. This second hypothesis is supported by the fact that depositions performed on ⟨100⟩-oriented silicon substrates always lead to heterogeneous, weakly-crystallized and non-aligned samples, as a consequence of the symmetry mismatch between the 3-fold ⟨001⟩ axis of $LiNbO_3$ and the 4-fold (100) Si symmetry.

The *c* lattice parameter deduced from the θ value of the (006) $LiNbO_3$ peak is 13.78 Å on Si and 13.81 Å on Al_2O_3, to be compared with 13.86 Å for the bulk material. This lower value could be explained by the existence of stresses at the interface between the films and the substrates. During the high-temperature deposition processes, the $LiNbO_3$ structure is strained because of the lattice mismatch but during cooling the films relax faster than the substrates because of the larger value of the linear thermal expansion coefficient in the (001) plane (Table II).

X-ray pole figures were measured using the reflection mode and projected on the surface of the samples. For both samples, they confirm the strong out-of-plane orientation of the crystallites, with a pole in the center of the $\{001\}$ pole figure (Fig. 2) reaching high density values of 23 mrd and 60 mrd (Multiple of a Random Distribution) for the Si-(111) and Al_2O_3-(001) samples respectively, showing that mainly all the crystallites have their *c*-axes perpendicular to the surface of the samples ($c_\perp$ orientation). However, a complete texturation could not be achieved neither on Si nor on Al_2O_3 substrates. Looking at the $\{100\}$ pole figures, one can see three other different

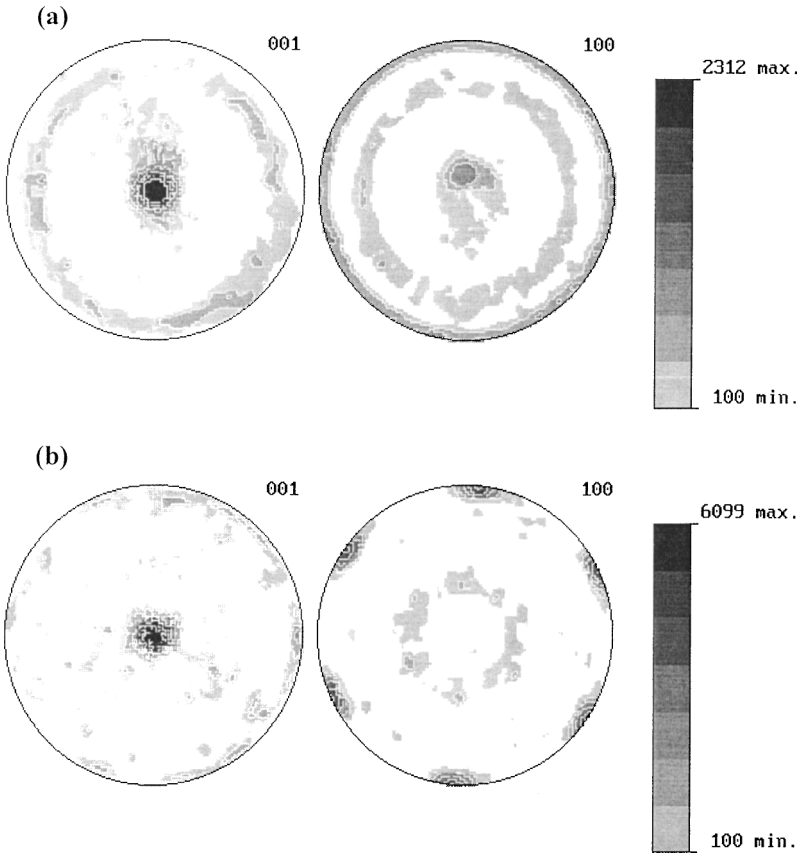

FIGURE 2 {001} and {100} pole figures, as recalculated from the orientation distribution function, of $LiNbO_3$ thin films deposited on **(a)** Si (111) and **(b)** Al_2O_3 (001) substrates. (Log.Scale; equal area projection)

out-of-plane texture components in our films. Firstly, in the film deposited on Si-(111), the {100} pole figure exhibits a marked reinforcement in its centre, synonymous of a $a_\perp$ orientation. The {001} pole figure of this sample shows also a ring centered at around 73° from the ⟨*c*⟩-axes, as a signature of a $\langle 202 \rangle_\perp$ orientation component. Secondly, in the film deposited on Al_2O_3-(001), a slightly reinforced ring is located at around 80° from the *c*-axes. This subsidiary component could be attributed to a $\langle 211 \rangle_\perp$ orientation.

The main differences between the two analyzed samples rely in their in-plane orientation pattern. The presence of a perfectly random in-plane

orientation (fiber texture) of the sample deposited on Si is clearly evidenced by the homogeneous rings in its {100} pole figure. The difference in lattice spacings and absence of coincidence site lattice explains this axially symmetric texture (Fig. 2a). On the contrary, {100}, {012} and {104} pole figures clearly demonstrate the in-plane orientation of the layers deposited on Al_2O_3 substrates. Because $LiNbO_3$ has a 3 m crystal symmetry (space group R3c), a single crystal should present a threefold symmetry in the (χ, φ) scans. In the pole figures presented in Fig. 3, a set of 3 peaks, spaced by 120°, reveals the hetero-epitaxial growth of the layers: one part of the crystallites have their ⟨110⟩-direction parallel to the [110] direction of the substrate, as shown by the high values of the pole densities. However, an additional set of 3 peaks is observed, also presenting a 3-fold symmetry and separated by 60° from the other peaks. This result suggests the presence of 2 variants rotated by 60° (or, equivalently 180°) with respect to each other around the *c*-axis (namely, $c_{\perp 0}$ being in exact alignment with the substrate and $c_{\perp 60}$). The volumic ratio of crystallites of each orientation is almost the same and experiments are still in progress to determine the influence of the thickness of both the sputtered and pyrosol-deposited layers on the final orientation components of the films.

The presence of 2 in-plane variants in hetero-epitaxial $LiNbO_3$ films deposited onto Al_2O_3 substrates has already been observed and discussed by several authors. In particular, the 60° variant is thought to be partially strain/stress-driven and, therefore, influenced by the lattice mismatch between the two materials [25]. Even though $LiNbO_3$ and Al_2O_3 are commonly indexed using the hexagonal notation, they are really trigonal (R3c and $R\bar{3}c$, respectively) and have only 3-fold symmetry. The 60°-rotated grains can easily be shown to have a higher cation alignment ordering energy compared to the 120°-rotated grains because of the reduced distance between Al, Li and Nb at the interface [26]. However, if the adsorbed atoms or adsorbed molecules do not have a sufficient mobility to move very far on the growth interface, they may be incorporated into an appropriate low energy site unless they arrive near it. Thus, the growth from these two different nuclei would result in two crystallographic variants in the films. An alternative explanation of the presence of two texture components consists in assuming the growth of crystallites with their *c*-axes in opposite direction with respect to one another. Thus, the observed structure could be due to the interplay between relaxation by misfit dislocations at the deposition temperature and relaxation by poly-domain formation during cooling. In other words, the two crystallographic variants could be compared to parallel and anti-parallel

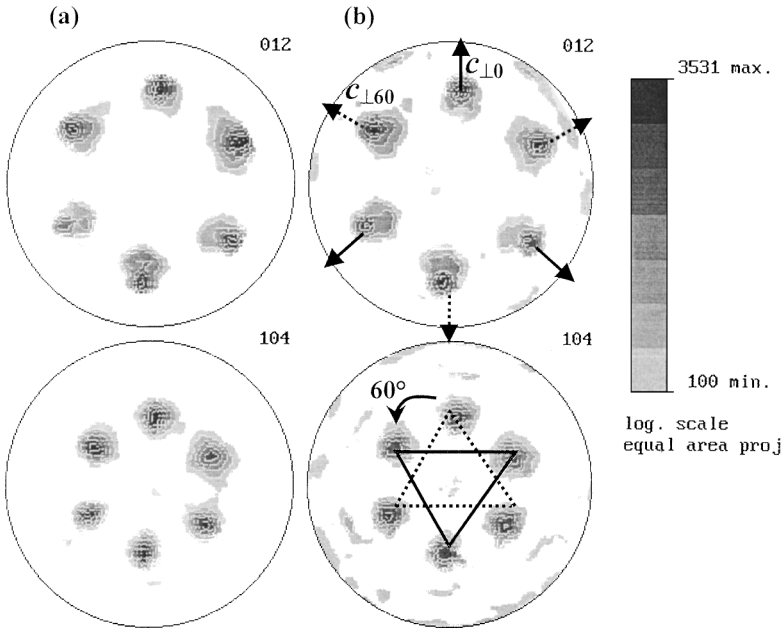

FIGURE 3 **(a)** Experimental and **(b)** recalculated {012} and {104} pole figures of a $LiNbO_3$ thin films deposited on Al_2O_3 (001) substrate. Note the good reproduction of the experimental pole figure, which shows the correctness of the refinement procedure. (Log.Scale; equal area projection)

domains. In the case of such a 50% "up" –50% "down" domain distribution, the macroscopic ferroelectric response should be 0, which would not be for another ratio. Experiments are still in progress to (un)validate this last hypothesis.

Both $LiNbO_3$/Si and $LiNbO_3/Al_2O_3$ heterostructures exhibit dense, homogeneous, columnar (Figs. 4 and 5). Using this refined growth process, final roughness as low as 8–10% and 5–7% to the total film thickness could be obtained onto Si and Al_2O_3 substrates, respectively. Both the average grain size and surface roughness increase on Si in comparison with Al_2O_3. The lattice mismatch and difference of structure between $LiNbO_3$ and Si create stresses within the films thus leading to grain boundary formation and grain boundary grooves which are significant contributors to grain growth and film roughening [27]. The use of semi-coherent interfaces, such as well-defined sapphire templates, allows a subsequent improve of the surface characteristics of the hetero-epitaxial films.

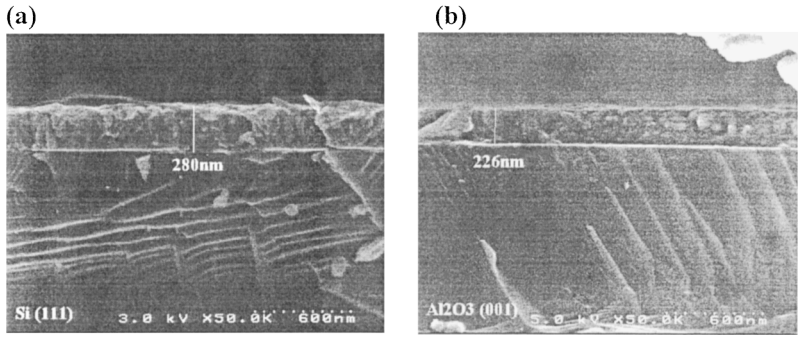

FIGURE 4 SEM micrographs of the cross-section of $LiNbO_3$ thin films deposited by the combined-deposition process on **(a)** Si (111) and **(b)** Al_2O_3 (001) substrates.

Surface Acoustic Wave Characteristics

In order to determine the SAW propagation characteristics for both $LiNbO_3$(001)/Si(111) and $LiNbO_3$(001)/Al_2O_3(001) heterostructures, we have taken advantages of a simulation software based on the Fahmy and Adler method [17] and adapted to layered structures. The film thickness (h) to acoustic wave frequency (f) product is commonly used to characterize the acoustic velocity and the electro-mechanical coupling coefficient. First theoretical results are shown in Fig. 6, pointing out the effect of an underlying epitaxially-matched substrate. The black and gray dash exponential-decay

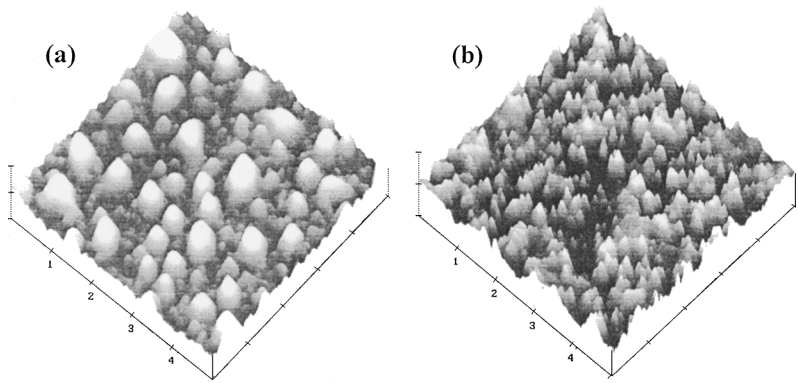

FIGURE 5 AFM micrographs of 300 nm-thick $LiNbO_3$ thin films deposited by the combined-deposition process on **(a)** Si (111) and **(b)** Al_2O_3 (001) substrates. (scale: $X \rightarrow 1$ μm/div; $Y \rightarrow 150$ nm/div)

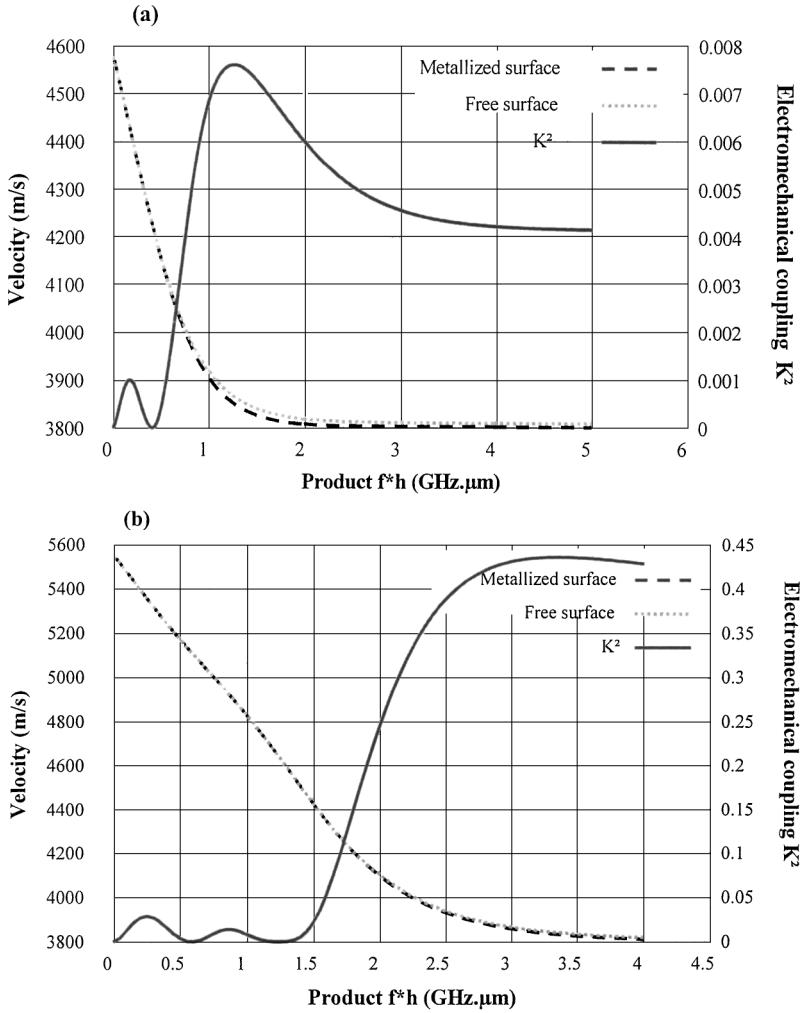

FIGURE 6 Velocity dispersion versus ($f * h$) for the Rayleigh mode of **(a)** $LiNbO_3$ (001)/Si (111) and **(b)** $LiNbO_3$ (001)/Al_2O_3 (001) heterostructures.

curves represent the Rayleigh mode velocities (the most relevant SAW mode) in the metallized (V_s) and free (V_f) surfaces, respectively. For a same ($f \times h$) product (from 0.01 to 0.4), V_s is strongly influenced by that of the substrate, ranging from 4600 m/s to 3800 m/s on Si (Fig. 6a) and from 5600 m/s to 3800 m/s on Al_2O_3 (Fig. 6b). The values of $LiNbO_3$(001)/Al_2O_3(001)

heterostructures are bigger than those measured in $LiNbO_3$ single crystals (typically, 4000 m/s to 3400 m/s) because of the effect of the sapphire substrate (around 5700 m/s) [28]. Indeed, when a piezoelectric film, such as $LiNbO_3$, is deposited on a non-piezoelectric substrate with a higher acoustic velocity, such as Al_2O_3, the velocity of the surface wave propagating through this layered structure ($LiNbO_3 + Al_2O_3$) will lie between that of the individual surfaces of $LiNbO_3$ and Al_2O_3.

In both cases, as ($f \times h$) increases, the velocity decreases. Thus, to obtain high-frequency SAW filters, the thickness of the $LiNbO_3$ films has to be as small as possible. But the efficiency of the electromechanical coupling between the input electrical signal and the generated surface acoustic wave decreases with decreasing $LiNbO_3$ film thickness (black continuous line in Fig. 6). For a high-frequency low-loss SAW device design, a trade-off between the operating frequency and the electromechanical coupling coefficient will have to be taken into account. As K^2 is linked to the acoustic velocity by the general equation $K^2 = \{2(V_{f-}V_s)/V_s\}$ [29], higher coupling constants are expected on Al_2O_3, with values as high as 45%. The frequency response of a 300 nm-thick $LiNbO_3$/Si system is shown in Fig. 7. The measured dispersion spectrum indicates a frequency center of 430 MHz, resulting in a surface wave velocity close to 4500 m/s. The asymmetry observed in the SAW signal can be easily explained by the variation of velocity as a function of frequency (Fig. 6a). The acoustic velocity varies with the product ($f \times h$)

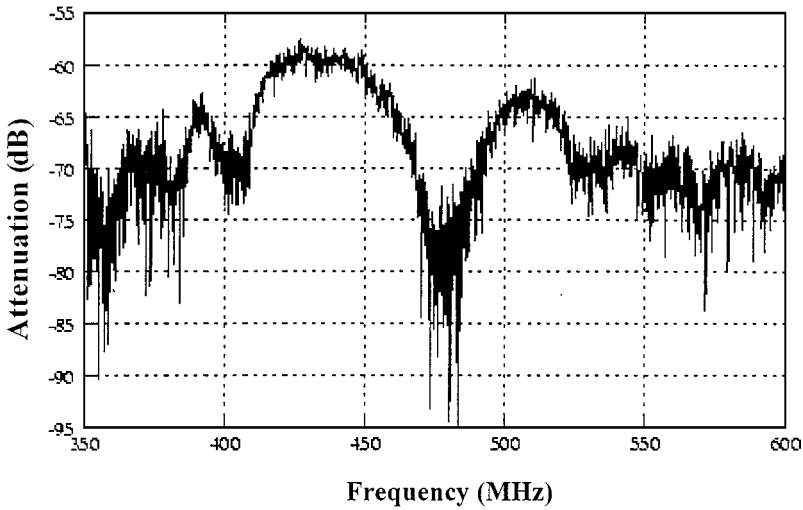

FIGURE 7 Experimental frequency response of a SAW signal on $LiNbO_3$/Si.

(where h is assumed to be constant), thus evidencing dispersion phenomena. The signal is strongly attenuated. Despite the strong out-of-plane orientation of the crystallites with their c-axis normal to the surface of the substrate, the wave is likely degraded because of the lack of in-plane organization in such as-deposited films. Both grain boundaries and misoriented grains act as highly diffusive planes increasing the losses of the waveguides. Then, for technical applications, the hetero-epitaxial nature (full texturation) of the films is required. Experiments are still in progress on Al_2O_3 substrates.

CONCLUSION

In this work, an original 2-step growth process and its successful application for the deposition of $LiNbO_3$ thin films has been demonstrated. This refined deposition technique results in highly c-oriented $LiNbO_3$/Si(111) and $LiNbO_3/Al_2O_3$(001) heterostructures with reduced surface roughness and fine columnar microstructures. If the former film only exhibits a fiber texture, the latter well evidences a marked in-plane organization of the crystallites with two separated main components. Thus, this method appears as very promising and effective for the deposition of high-quality thin films for SAW applications.

A simulation of the Rayleigh SAW velocity V_s and coupling coefficient K^2 has been carried out. Theoretical results show the potential usefulness of oriented $LiNbO_3$/Si and $LiNbO_3/Al_2O_3$ heterostructures. First experimental measurements on $LiNbO_3$/Si systems reveal high insertion losses, resulting from the lack of coherent interface between the two materials. Works are still in progress to determine the SAW characteristics of $LiNbO_3/Al_2O_3$ samples. Improvements of the overall film texture and, in particular, deposition of well in-plane organized materials should provide efficient films for the transfer of acoustic waves in SAW devices.

The authors wish to thank Dr M. Ramonda for AFM measurements and Dr S. Ballandras and Dr T. Pastureaud for SAW modeling.

REFERENCES

[1] G. Peterson, A. Ballman, P. Lenzo, and M. Bridenbaugh, *Appl. Phys. Lett.* **5**, 62 (1964).
[2] G. Boyd, R. Miller, K. Nassau, W. Bond, and A. Savage, *Appl. Phys. Lett.* **5**, 234 (1964).
[3] R. Miller, G. Boyd, and A. Savage, *Appl. Phys. Lett.* **6**, 77 (1965).
[4] E. Spencer, P. Lenzo, and K. Nassau, *Appl. Phys. Lett.* **7**, 67 (1965).
[5] A. W. Warner, M. Onoe, and G. A. Coquin, *J. Acoust. Soc. Am.* **42**, 1223 (1967).
[6] R. S. Weis and T. K. Gaylord, *Appl. Phys. A* **37**, 191 (1985).

[7] Y. Furushima, T. Nishida, M. Shimizu, and T. Shiosaki, *1993 IEEE Ultrason. Symp. Proc.* 263 (1993).
[8] Y. Shibata and T. Kawai, *Jpn. J. Appl. Phys.* **34**, 249 (1995).
[9] D. F. Fork, F. Armani-Leplingard, and J. J. Kingston, *Mat. Res. Soc. Bull.* **7**, 53 (1996).
[10] D. Royer and E. Dieulesaint, *Ondes élastiques dans les solides*, **Tome 2** (Masson, Paris, 1996) 127p.
[11] V. Bornand, I. Huet, Ph. Papet, and E. Philippot, *Annales de Chimie—Sciences des Matériaux* (2001).
[12] I. Huet, V. Bornand, and Ph. Papet, submitted to Thin Solid Films.
[13] D. Chateigner, P. Germi, and M. Pernet, *Mater. Sci. For.* **157–163**, 1379 (1994).
[14] J. Ricote and D. Chateigner, *Bol. Soc. Esp. Ceram. Vidrio* **38**, 587 (1999).
[15] D. Chateigner, *Etude de la texture cristallographique de céramiques et de couches minces supraconductrices YbaCuO en relation avec les propriétés physiques* (in French/Thesis of the J.F. University, Grenoble, 1994) 135p.
[16] H.-R. Wenk, S. Matthies, J. Donovan, and D. Chateigner, *J. Appl. Cryst.* **31**, 262 (1998).
[17] A. H. Fahmy and A. L. Adler, *Appl. Phys. Lett.* **22**, 495 (1973).
[18] E. L. Adler, *IEEE Trans. on Ultrasonics, Ferroelectrics and Frequency Control* **37**, 485 (1990).
[19] G. E. Peterson and P. M. Bridenbaugh, *J. Chem. Phys.* **48**, 3402 (1968).
[20] J. R. Carruthers, G. E. Peterson, and M. Grasso, *J. Appl. Phys.* **42**, 5 (1971).
[21] F. K. Lotgering, *J. Inorg. Nucl. Chem.* **9**, 113 (1959).
[22] H. Yoshiyama, S. Tanaka, Y. Hikami, S. Ohshio, J. Nishiura, H. Kawakami, and H. Kobayashi, *J. Cryst. Growth* **86**, 56 (1988).
[23] N. Fujimura, T. Nishihara, S. Goto, J. Xu, and T. Ito, *J. Cryst. Growth* **130**, 269 (1993).
[24] E. I. Givargizov, *Oriented crystallization on amorphous substrates* (Plenum Press, New York, 1991) 370p.
[25] T. A. Derouin, C. D. E. Lakeman, X. H. Wu, J. S. Speck, and F. F. Lange, *J. Mater. Res.* **12**, 1391 (1997).
[26] J. Guo, D. E. Ellis, and D. J. Lam, *Phys. Rev. B* **45**, 13647 (1992).
[27] D. K. Fork, F. Armani-Leplingard, J. J. Kingston, and G. B. Anderson, *Mater. Res. Symp. Proc.* **392**, 189 (1985).
[28] W. M. Yim and R. J. Paff, *J. Appl. Phys.* **45**, 1456 (1974).
[29] I. A. Borodina, S. G. Joshi, B. D. Zaitsev, and I. E. Kuznetsova, *Acous. Phys.* **46**, 33 (2000).